

Evolution of fabric anisotropy in cyclic liquefaction of sands

Jiangtao Wei and Gang Wang*

*Department of Civil and Environmental Engineering
The Hong Kong University of Science and Technology
Clear Water Bay, Kowloon, Hong Kong
gwang@ust.hk

Received 5 October 2016
Accepted 18 October 2016
Published 24 November 2016

Abstract Cyclic liquefaction of sands is influenced by many factors including the initial fabric. Yet, it is difficult to quantify the soil fabric using laboratory technology. In this study, discrete element method (DEM) is used to numerically simulate the process of liquefaction under undrained cyclic loading. Samples with the same void ratio and varying degrees of fabric anisotropy are prepared by the pre-shearing method. Fabric evolution before and after cyclic liquefaction is quantified by the coordination number, angular distribution and the principal direction of inter-particle contacts. The DEM study demonstrated that the coordination number decreases and the fabric anisotropy increases gradually when the sand is cyclically sheared to approach the initial liquefaction. In this process, the principal direction of the anisotropic fabric tensor is not coaxial with the stress tensor. After initial liquefaction, all samples with different initial fabric evolve towards a same fabric, which is strongly anisotropic. The principal direction of the fabric aligns with the principal direction of the stress in the post-liquefaction stage.

Keywords DEM; fabric anisotropy; liquefaction; initial fabric.

1. Introduction

Liquefaction of sandy soils has caused significant damage to infrastructure during past earthquakes, including loss of bearing capacity of soil foundation, excessive deformation and large lateral spreading of the ground [Ye and Wang, 2015, 2016; Ye *et al.*, 2016]. The state-of-the-art framework for liquefaction triggering and post-liquefaction deformation have been based on simple indices, such as the void ratios or standard penetration tests and applied loading conditions [Idriss and Boulanger, 2008; Wang and Xie, 2014].

Yet, granular materials such as sands are collections of a large number of discrete particles, which behave differently than solids, liquids and gases, and shall be treated as a new form of matter. A number of laboratory tests demonstrated that liquefaction resistance of sands is also closely related to their initial fabrics [Finn *et al.*, 1970;

*Corresponding author.

Ishihara and Okada, 1978; Nemat-Nasser and Tobita, 1982; Suzuki and Toki, 1984; Ye *et al.*, 2015]. Here, “fabric” represents arrangement of particles, particle groups and voids in the granular packing [Sitar, 1983]. Different initial fabrics of soils can be induced by different preparation methods (e.g., dry deposition versus moist temping) or pre-shearing histories [Mulilis *et al.*, 1977; Ishihara and Okada, 1978; Vaid *et al.*, 1989; Ishibashi and Capar, 2003; Yimsiri and Soga, 2010; Sze and Yang, 2013]. However, it is difficult to quantify the soil fabric using existing laboratory technique.

Numerical simulation, such as the discrete element method (DEM), provides a viable mean to quantify the soil fabric because all particles and inter-particle contacts can be realistically simulated such that small scale information of particles and voids can be used to quantify the fabric. Recent DEM simulation by Wei and Wang [2016] established the relationship between the initial fabric and liquefaction resistance of sands, which corroborated laboratory test results. In this study, the DEM simulation is used to study evolution of the fabric in the sand packings during cyclic loading. In the following sections, the DEM simulation is first introduced. Then, indicators to quantify the fabric are formulated based on the number and angular distribution of inter-particle contacts. After samples with different initial fabrics are generated by the pre-shearing method, cyclic simple shear tests are performed to load the samples to liquefaction. Finally, evolution of the fabric in sands before and after cyclic liquefaction is compared, followed by conclusions and discussions.

2. Numerical Simulation

2.1. Samples generation with different initial fabric

Yade [Šmilauer *et al.*, 2010] is used to perform the DEM numerical simulation. A total number of 10,000 spherical particles are generated in the cubical packing with the periodic boundary as shown in Fig. 1(a). The radius of particle is ranging from 0.15 mm to 0.45 mm. Particle density is 2650 kg/m³, which is close to the actual density of the sand grain. The use of spherical particles eliminates contribution of particle shape to the fabric anisotropy. The Hertz–Mindlin model is used to calculate the inter-particle contact force, as illustrated in Fig. 1(b).

The normal contact force is given by

$$f_n = k_n \delta, \quad (1)$$

where $k_n = \frac{2E}{3(1-\nu^2)}\sqrt{r}$, and r is the equivalent radius determined by the radii of two particles (r_A and r_B) in contact: $r = \frac{r_A r_B}{r_A + r_B}$; δ is the overlapping of a pair of particles in contact. E and ν are Young’s modulus and Poisson’s ratio of particles, respectively. In the simulation, $E = 70$ GPa and $\nu = 0.3$.

The tangential contact force is given by

$$df_s = k_s dU_s, \quad (2)$$

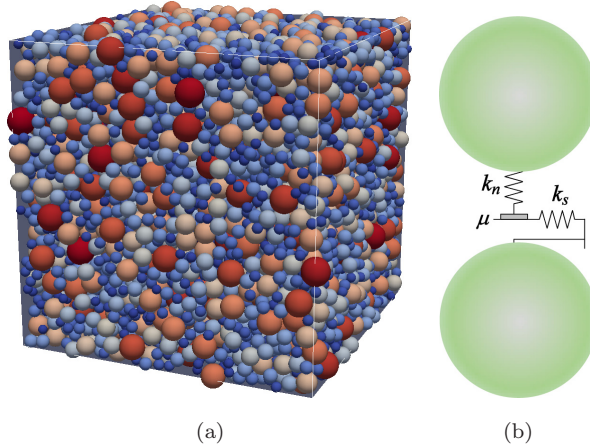


Fig. 1. DEM numerical simulation (a) granular packing and (b) inter-particles contact force model.

where $k_s = \frac{2E\sqrt{r}}{(1+\nu)(1-\nu)}\sqrt{\delta}$, U_s is the tangential displacement of the contact. In addition, the tangential force is restricted by a maximum allowable value $f_{s,\max}$:

$$f_{s,\max} = \mu f_n, \quad (3)$$

where μ is the frictional coefficient of particle. When tangential force reaches the maximum allowable value, contact sliding occurs. During the cyclic loading after sample generation, frictional coefficient of all particles is set to be 0.5.

In the numerical simulation, the pre-shearing method proposed by Yimsiri and Soga [2010] is used to generate packing with different initial fabric but with the same void ratio under the same confining pressure. The procedure of the pre-shearing method is illustrated in Fig. 2(a). Firstly, the samples were isotropically consolidated under the confining pressure of 100 kPa. Then, drained triaxial compression was performed on the samples to induce the anisotropic fabric (more contact normals were oriented along the compression direction). At the end, the samples were reconsolidated under hydrostatic pressure $p_0 = 100$ kPa. The prepared sample was then subjected to undrained cyclic simple shear as shown in Fig. 2(b).

2.2. Quantification of fabric based on particle contacts

Coordination number measures the average number of inter-particle contacts for each particle in the granular packing. It is the most basic contact-scale indicator to quantify fabric of sands, and it can be easily obtained from DEM simulation [O'Sullivan, 2011]. It is simply defined as the ratio between the number of inter-particle contacts and the number of particles:

$$Z = \frac{2N_c}{N_p}, \quad (4)$$

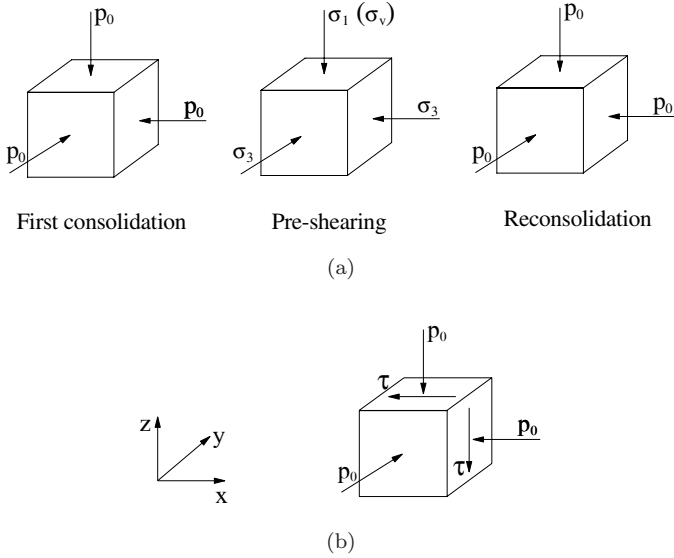


Fig. 2. (a) Pre-shearing method to generate samples and (b) cyclic simple shear test.

where N_c is the number of total contacts and N_p is the number of total particles. The coefficient 2 is due to the fact that each contact is shared by two particles. In the granular packing, particles can be divided into rattlers and non-rattlers. Rattlers refer to particles that have no contribution to the stable state of stress. Non-rattlers are the remaining particles in the packing that are involved in the force chain and contact force transmission. In the numerical simulation, particles with only one or no contact are regarded as rattlers since these particles cannot participate in the contact force transmission. Rattler fraction is defined as the ratio between the number of rattlers and the total number of particles [Bi *et al.*, 2011]:

$$f_R = (N_0 + N_1)/N_p, \quad (5)$$

where N_0 and N_1 are the number of particles with no contact and one contact, respectively.

Complementary to the coordination number, mechanical coordination number [Thornton, 2000] is defined as follows to measure the average number of contacts for non-rattlers:

$$Z_m = \frac{2N_c - N_1}{N_p - (N_0 + N_1)}, \quad (6)$$

where $2N_c - N_1$ is the number of contacts associated with non-rattlers, and $N_p - (N_0 + N_1)$ is the total number of non-rattlers. Z , Z_m and f_R can be related by the following equation:

$$Z = \frac{2N_c}{2N_c - N_1} Z_m (1 - f_R). \quad (7)$$

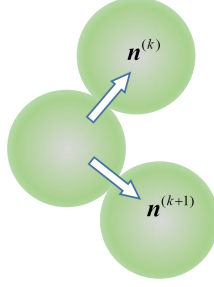


Fig. 3. Inter-particle contact direction.

To quantify the anisotropy of the contact based fabric, we adopt the second-order fabric tensor proposed by Satake [1982] and Oda [1972], which is defined as the following equation:

$$\phi_{ij} = \frac{1}{N_c} \sum_{k=1}^{N_c} n_i^{(k)} n_j^{(k)} = \int_{\Theta} E(\Theta) n_i n_j d\Theta, \quad (8)$$

where n is the orientation vector of the contact normal, shown in Fig. 3, and $E(\Theta)$ is the angular distribution of the contact normal, such that

$$\int_{\Theta} E(\Theta) d\Theta = 1.$$

Expanded using Fourier series and ignoring the higher-order terms [Sitharam *et al.*, 2009], $E(\Theta)$ can be written as

$$E(\Theta) = E_0(1 + a_{ij}n_in_j), \quad (9)$$

where a_{ij} is a symmetric second-order tensor that characterizes the anisotropy of fabric tensor. Substituting $E(\Omega)$ in Eq. (9) to Eq. (8), the relationship $a_{ij} = \frac{15}{2}\phi'_{ij}$ can be determined for a 3D case, where ϕ'_{ij} is the deviatoric part of the fabric tensor ϕ_{ij} . We use the following invariant of a_{ij} to quantify the anisotropy degree of the fabric tensor,

$$a_c = \sqrt{\frac{3}{2}(a_{ij}a_{ij})}. \quad (10)$$

In the case of simple shear loading shown in Fig. 2(b), the stress tensor and the fabric tensor can be written as follows:

$$\sigma_{ij} = \begin{bmatrix} p_0 & 0 & \tau_{xz} \\ 0 & p_0 & 0 \\ \tau_{zx} & 0 & p_0 \end{bmatrix}; \quad \phi_{ij} = \begin{bmatrix} \phi_{xx} & 0 & \phi_{xz} \\ 0 & \phi_{yy} & 0 \\ \phi_{zx} & 0 & \phi_{zz} \end{bmatrix}. \quad (11)$$

Note that some components of the fabric tensor are approximated to be zero. The major and minor eigenvalues of the fabric tensor are:

$$\Phi_1, \Phi_3 = \frac{1}{2}(\phi_{xx} + \phi_{zz}) \pm \frac{1}{2}\sqrt{(\phi_{xx} - \phi_{zz})^2 + 4\phi_{xz}^2}. \quad (12)$$

The major principal direction of the fabric tensor is:

$$\mathbf{n}_1 = (\cos \theta_1 \quad 0 \quad \sin \theta_1)^T, \quad (13)$$

$$\tan 2\theta_1 = \frac{2\phi_{xz}}{\phi_{xx} - \phi_{zz}}, \quad (14)$$

where θ_1 is the angle between \mathbf{n}_1 and x -axis. The major principal direction shows the orientation of the maximum concentration of contact normals. In the following sections, coordination number Z , anisotropy degree a_c and major principal direction of the fabric θ_1 are adopted to quantify the fabric evolution.

2.3. Initial fabric characterization of different samples

As summarized in Table 1, eight samples are prepared by the pre-shearing method (termed as S1 to S8), in addition to one isotropic sample (termed as ISO) prepared without pre-shearing. For sample S1 to S8, different initial fabrics are achieved. One may refer to Wei and Wang [2016] for more details of the samples generation. All the samples have almost identical void ratio of around 0.611–0.612. These samples can be categorized as a medium dense sand since the relative density is about 0.56 (the maximum and minimum void ratio are 0.759 and 0.497, respectively).

To quantitatively compare the initial fabric of these samples, we check the fabric indicators of these samples and the results are demonstrated in Fig. 4. Sample ISO has the lowest anisotropy degree $a_c = 0.038$. From S1 to S8, anisotropy degree of initial fabric increases from 0.15 to 0.38. For these samples, the anisotropy of initial fabric is due to the concentration of inter-particle contacts along the compression direction. Therefore, the principal directions of initial fabrics are all close to 90° , which is aligned with the compression direction during pre-shearing.

Coordination numbers Z of these samples are presented in Fig. 4(c). Sample ISO has the highest coordination number of 3.77. For S1–S8, coordination number decreases from 3.57 to 2.51. The mechanical coordination number Z_m and rattler fraction f_R of these samples are demonstrated in Fig. 4(d). Z_m decreases from 5.05 in sample ISO to 3.95 in sample S8. For a stable 3D granular packing, Z_m

Table 1. Different initial fabric of the samples.

Sample	Void ratio	Initial fabric	
		Z	a_c
ISO	0.6115	3.769	0.038
S1	0.6114	3.572	0.153
S2	0.6112	3.405	0.223
S3	0.6118	3.283	0.289
S4	0.6112	3.105	0.335
S5	0.6119	2.933	0.350
S6	0.6119	2.823	0.376
S7	0.6112	2.640	0.362
S8	0.6114	2.518	0.385

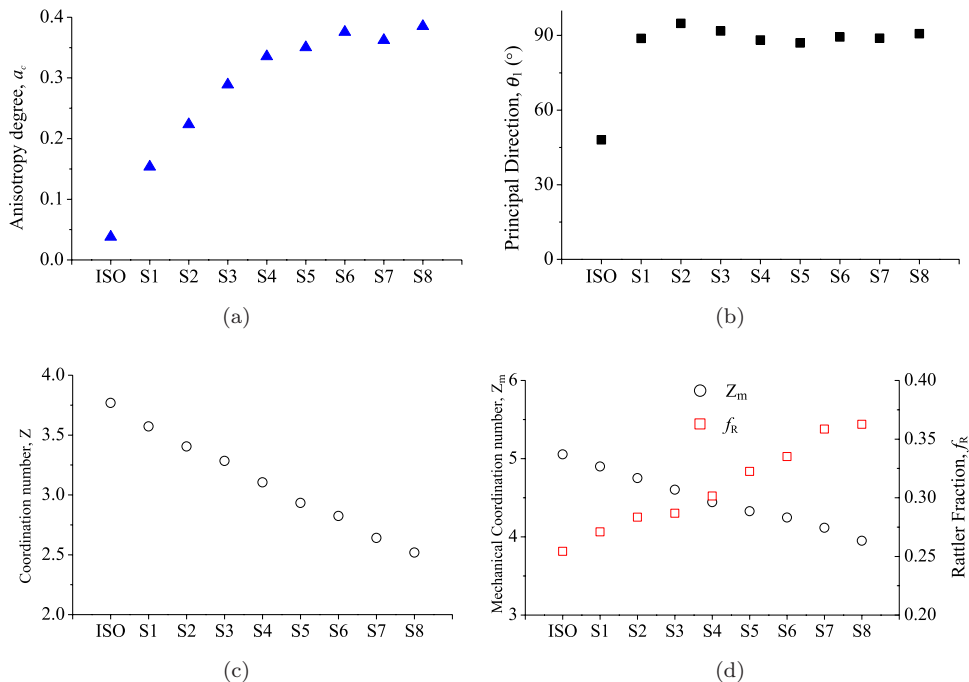


Fig. 4. Initial fabric of different samples. (a) Total anisotropy degree a_c ; (b) major principal direction θ_1 ; (c) coordination number Z and (d) mechanical coordination number Z_m and rattler fraction f_R .

should be larger than 4 [Edwards, 1998]. We observed that only Z_m in sample S8 is slightly below 4. In the cyclic simple shear simulation, S8 is very easy to liquefy and has the lowest liquefaction resistance. Compared with Z_m , rattler fraction f_R of these samples has an opposite trend such that f_R increases from 0.254 in sample ISO to 0.363 in sample S8. It means that if the sample has higher degree of fabric anisotropy, fewer particles in the sample will contribute to the force chain.

3. Cyclic Simple Shear Tests

After the generation of samples with different fabrics, undrained cyclic simple shear loading is performed to these samples to study the fabric evolution during the liquefaction process. Simulation results from sample S2 and S6 are presented, as shown in Fig. 5, to be the representatives. Cyclic stress ratio (CSR) in the figure is defined as the cyclic shear stress (τ_{xz}) acting on horizontal plane divided by the vertical effective stress ($\sigma'_v = 100$ kPa), $CSR = \tau_{xz}/\sigma'_v$. With the increase of cycle numbers, vertical effective stress (σ'_v) gradually decreases until initial liquefaction occurs. The initial liquefaction is based on the occurrence of zero vertical effective stress, in practice, $\sigma'_v < 0.5$ kPa. After liquefaction, stress path shows repeated “butterfly” loops while the shear strain amplitude keeps increasing cycle by cycle. Note that

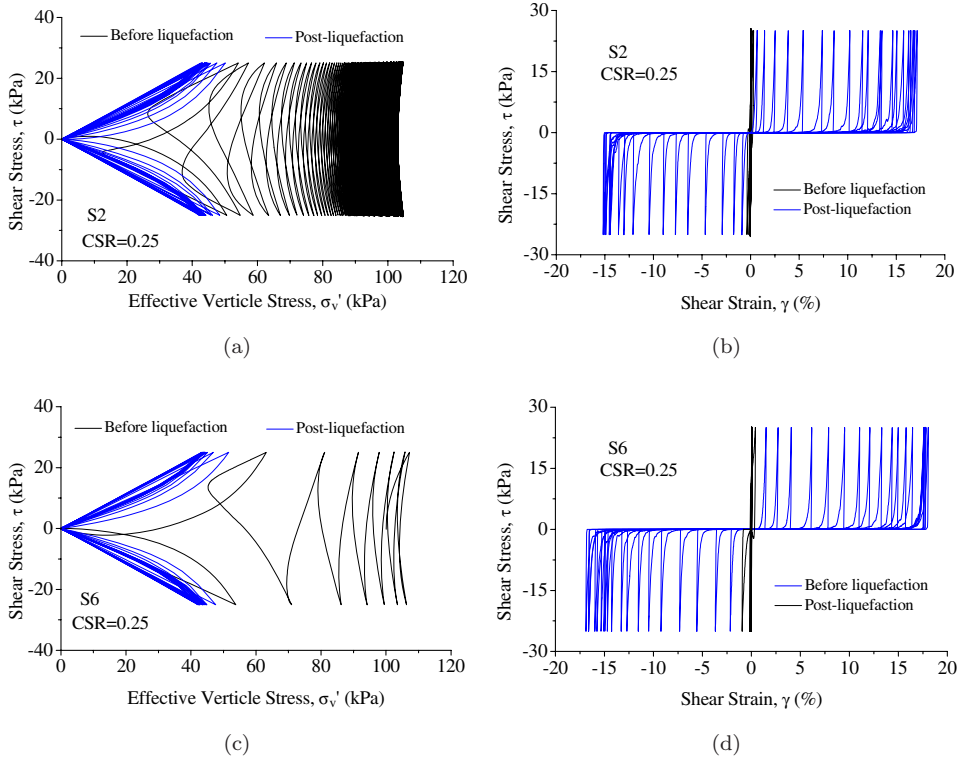


Fig. 5. Mechanical behaviors of samples during undrained cyclic simple shear loading with CSR = 0.25. (a) Stress path of sample S2; (b) stress strain curve of sample S2; (c) stress path of sample S6 and (d) stress strain curve of sample S6.

samples S2 and S6 show symmetric cyclic stress and strain although the initial fabric is anisotropic. It is because the cyclic shear stress applied is symmetric and is perpendicular to the direction of the initial fabric. Figure 6 shows the evolution of shear strain with the cycle number. In both samples S2 and S6, shear strain amplitude increases very slowly before liquefaction and starts to grow rapidly in the post-liquefaction stage. This observation is consistent with laboratory tests [Zhang and Wang, 2012].

Comparing the mechanical behaviors of sample S2 and S6, we can find a noticeable difference in terms of stress path before initial liquefaction. The result shows sample S2 has much higher liquefaction resistance compared with sample S6. Under the same cyclic shear stress (CSR = 0.25), S2 needs 250 loading cycles to liquefy. Yet, only seven loading cycles are needed for sample S6 to reach the initial liquefaction. The simulation results confirm the laboratory observations that initial fabric can significantly influence the liquefaction resistance of sands [Suzuki and Toki, 1984; Oda *et al.*, 2001; Ye *et al.*, 2015]. Wei and Wang [2016] quantitatively studied the influence of initial fabric to liquefaction resistance and found the correlation

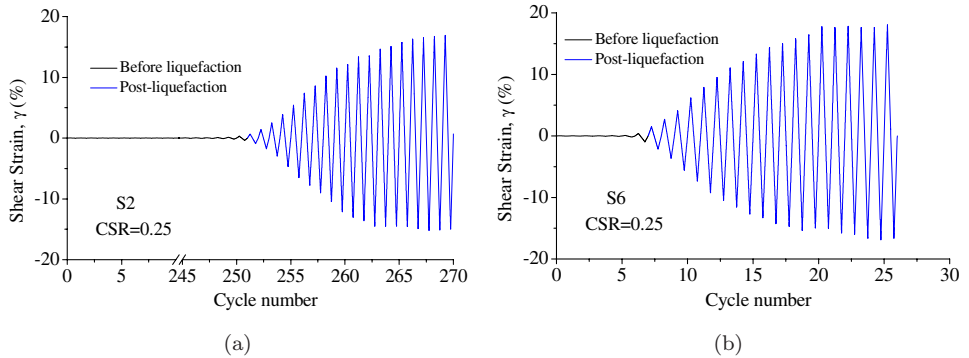


Fig. 6. The evolution of shear strain amplitude during undrained cyclic simple shear loading. (a) Sample S2 and (b) sample S6.

between the coordination number and liquefaction resistance. In post-liquefaction stage, sample S2 and S6 demonstrate similar behaviors that single amplitude of shear strain saturated at around 18% after about 20 cycles (counted from initial liquefaction).

4. Fabric Evolution During Cyclic Loading

4.1. Before initial liquefaction

During undrained cyclic loading, the decrease in effective stress reflects the change in the load-bearing structure of sands [Wang and Wei, 2016]. From the microscale perspective, inter-particle contacts will gradually reduce and this process is confirmed by the evolution of coordination number Z with effective vertical stress, σ'_v , as illustrated in Fig. 7. All samples start with the same stress state ($\sigma'_v = 100$ kPa) but a different Z . With the increase in cycle number, both σ'_v and Z gradually decrease. When σ'_v approaches zero (initial liquefaction), Z of all samples decreases to the same value that is between 1.5 and 2.0. It is not unexpected that samples with lower initial coordination numbers will reach initial liquefaction within a fewer number of loading cycles and has lower liquefaction resistance.

Reorientation of inter-particle contacts during cyclic loading is reflected by the evolution of the anisotropy degree a_c and the major principal direction θ_1 . Simulations from four samples (ISO, S1, S4 and S7) under $CSR = 0.25$ are taken as examples.

First, comparison of fabric indicators, a_c and θ_1 , between loading cycles is demonstrated in Fig. 8, where data are taken at the instance of reaching the maximum shear stress in each cycle. For the sample ISO with the isotropic fabric, anisotropy degree at maximum shear stress keeps increasing with the increase in loading cycles in Fig. 8(a). The major principal direction of the fabric remains

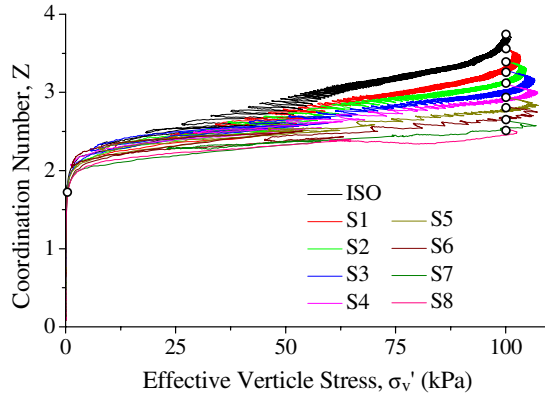


Fig. 7. Evolution of coordination number versus effective vertical stress before initial liquefaction.

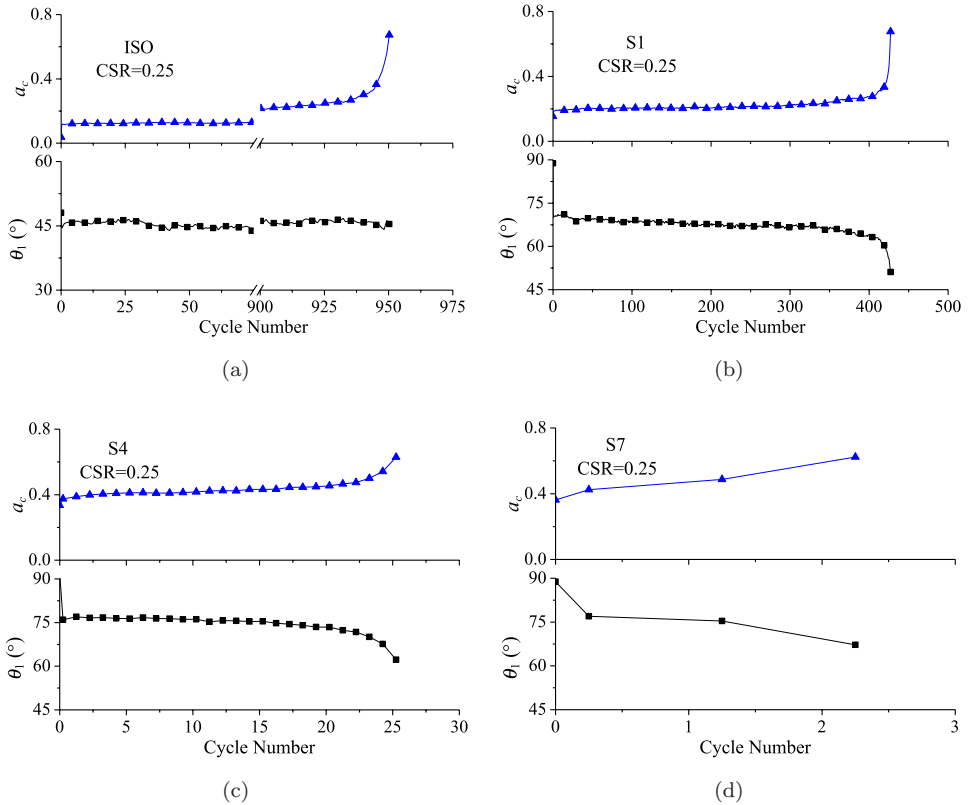


Fig. 8. The evolution of anisotropy degree and fabric direction between loading cycles before liquefaction. (a) Sample ISO; (b) sample S1; (c) sample S4 and (d) sample S7.

almost constant at around 45° , which is in line with the major principal stress direction. This indicates that the majority of inter-particle contacts are concentrated in the major principal stress direction.

Sample S1, S4 and S7 are all prepared with pre-shearing. In these three samples, S7 has the highest initial anisotropy degree of 0.362 and sample S1 has the lowest anisotropy degree of 0.153. As shown in Figs. 8(b)–8(d), anisotropy degree a_c of these three samples increases with the increase in cycle number before liquefaction. The increasing rate of a_c is very slow in most loading cycles and gradually speeds up in the last several cycles when granular packing is approaching initial liquefaction. This behavior is observed in all the samples. It reflects that fabric re-organization becomes more extensive when sample is approaching the initial liquefaction. The major difference in fabric evolution between these samples lies in the major principal direction. For these three samples, θ_1 rotates from initial 90° (vertical direction) to 75° during the first loading cycle and continues to rotate towards 45° with further loading cycles. The increasing rate of θ_1 is very slow until the sample approaches the initial liquefaction.

To check the evolution of fabric within the loading cycle, simulation results of two loading cycles in ISO and S4 are demonstrated in Fig. 9. For sample ISO during a half loading cycle (τ decreases from 25 kPa to -25 kPa), a_c firstly decreases from a peak value to a value close to zero and then increases to the peak value again. In a careful inspection, a_c reaches its peak value when the shear stress reaches its peak value ($\tau = \pm 25$ kPa). a_c reaches the minimum when τ is around zero. Meanwhile, the major principal direction θ_1 shows a sudden jump from 45° to 135° and vice versa when the sign of the shear stress changes. The major principal direction of stress is also plotted for reference.

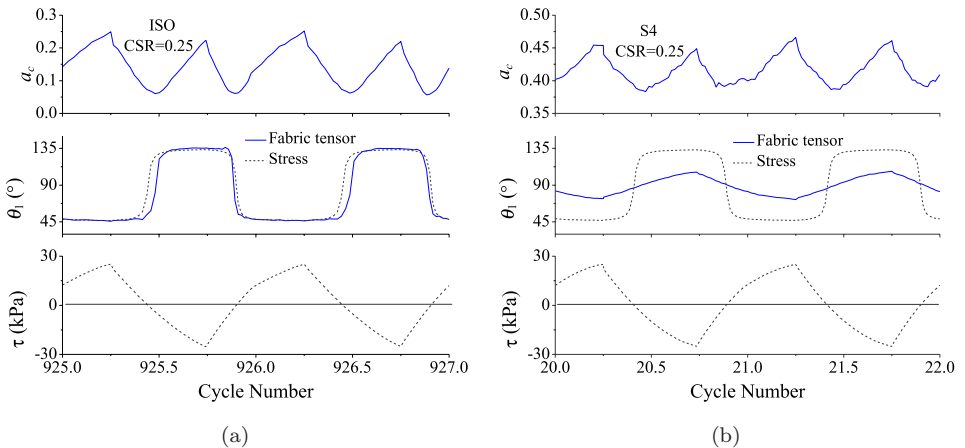


Fig. 9. Evolution of anisotropy degree and fabric direction within the loading cycle before liquefaction. Shear stress during the same cycle is plotted below for reference. (a) Sample ISO and (b) sample S4.

The evolution of θ_1 is notably different in sample S4. As shown in Fig. 9(b), θ_1 for S4 evolves gradually from 75° to 115° , in contrary to the sudden jump of θ_1 in sample ISO. The evolution of a_c for ISO and S4 has the same trend, but different lower bounds. For sample S4, the minimum a_c (0.37) is still much higher than that in ISO. By combining the evolution of fabric between and within loading cycles, we can get a better picture of fabric evolution before liquefaction: anisotropy degree increases when loading cycle increases in an oscillated pattern. The fabric direction rotates almost symmetrically around the initial fabric direction (90°) within each loading cycle and the rotation angle gradually increases as cycle number increases.

4.2. The post-liquefaction stage

In the post-liquefaction stage, the evolution of fabric between loading cycles is firstly demonstrated in Fig. 10. All the data are taken at the state of the maximum shear stress of 25 kPa in each loading cycle after liquefaction. Cycle number in the figure is counted only after the initial liquefaction. In the post-liquefaction stage, evolution of anisotropy degree a_c is quite similar for all samples such that a_c increases at the first eight cycles and stabilizes at 1.35 in the subsequent loading cycles. The fabric direction θ_1 of ISO remains to be 45° , which is in line with the major principal direction of stress. For other samples S1–S8, the fabric direction rotates dramatically in the first four cycles and converges to 45° in the end. It indicates that all samples with different initial fabric evolve towards the same fabric in post-liquefaction stage. This explains why the post-liquefaction behaviors of these samples are quite similar.

The data of five cycles before initial liquefaction are also presented in Fig. 10 to demonstrate the fabric evolution close to the initial liquefaction. During these loading cycles, both a_c and θ_1 demonstrate a rapid change, indicating intensive fabric adjustment of granular packing close to the initial liquefaction.

Within the loading cycle, granular packing will experience the “flow stage” (effective stress is almost zero) and “hardening stage” (effective stress starts to

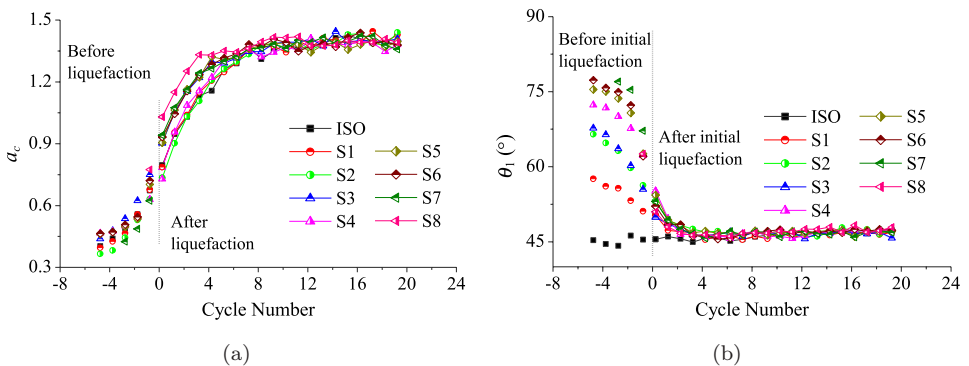


Fig. 10. Fabric evolution in different samples in the post-liquefaction stage. (a) Anisotropy degree a_c and (b) fabric direction θ_1 .

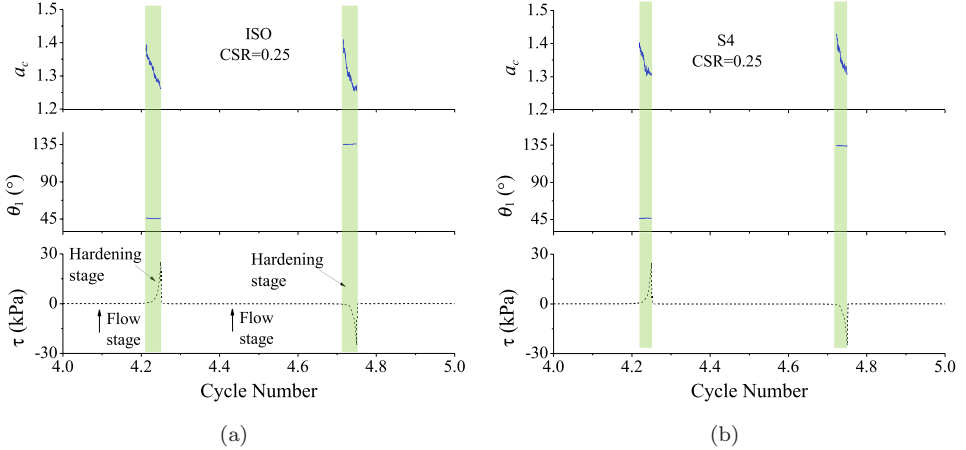


Fig. 11. Evolution of anisotropy degree and fabric direction within the loading cycle after liquefaction. (a) Sample ISO and (b) sample S4. Only data in the hardening stage (highlighted) is shown.

grow rapidly). One characteristic of fabric during “flow stage” is that the total number of inter-particle contact can be very low and the load-bearing structure is not fully established [Wang and Wei, 2016]. Therefore, only the evolution of fabric during the “hardening stage” is demonstrated in Fig. 11. For both samples ISO and S4, anisotropy degree a_c shows a slight decrease from 1.40 (at the beginning of the “hardening stage”) to 1.30 (at the maximum shear stress), which means the re-established fabric is highly anisotropic. Meanwhile, the major principal direction θ_1 is around 45° or 135° , which is completely aligned with the principal direction of the stress.

5. Conclusions

Fabric evolution in sands with different initial fabric is explored using DEM simulation. Based on pre-shearing method, samples with the same void ratio and confining pressure but different initial fabric are generated. The fabric of sands is quantified by the coordination number Z and contact-based fabric tensor. Anisotropy degree a_c and fabric direction θ_1 are further derived from the fabric tensor to characterize the angular distribution of contact normals. For samples prepared with pre-shearing, contact normals before the cyclic loading are concentrated along the vertical direction ($\theta_1 = 90^\circ$). Compared with the sample with the isotropic fabric, samples with a higher degree of anisotropy a_c have a lower coordination number Z .

The results from numerical simulation well capture the sand behaviors during undrained cyclic loading. Before liquefaction, samples with different initial fabrics demonstrate significantly different cyclic behaviors (e.g., stress path) and fabric evolution. Characteristics of fabric evolution during liquefaction process can be

summarized below:

- (1) Coordination number Z of initial fabric varies significantly from sample ISO ($Z = 3.769$) to sample S8 ($Z = 2.518$). However, upon initial liquefaction, Z of all samples decreases to about the same value (between 1.5 and 2.0).
- (2) Initial anisotropy degree a_c varies from close to zero (0.038) in sample ISO to a high value in sample S8 (0.385). a_c increases with increasing number of loading cycles following an oscillated pattern.
- (3) The fabric direction θ_1 rotates around the initial fabric direction (90°) within each loading cycle, and the rotation angle gradually increases as cycle number increases.

In the post-liquefaction stage, fabrics of all samples converge to the same state within a few loading cycles. Fabric direction θ_1 is coaxial with the principal stress direction and the anisotropy degree a_c at the maximum shear stress ($\tau = 25$ kPa) reaches a highly anisotropic steady value of (1.35). In other words, the influence of the initial fabric is “wiped out” when soils liquefied.

Acknowledgments

The study is financially supported by Theme-based Research Scheme Grant No. T22-603/15N from Hong Kong Research Grants Council.

References

- Bi, D., Zhang, J., Chakraborty, B. and Behringer, R. P. [2011] “Jamming by shear,” *Nature* **480**(7377), 355–358.
- Finn, W., Bransby, P. L. and Pickering, D. J. [1970] “Effect of strain history on liquefaction of sand,” *Journal of the Soil Mechanics and Foundations Division* **96**(6), 1917–1934.
- Ishibashi, I. and Capar, O. F. [2003] “Anisotropy and its relation to liquefaction resistance of granular material,” *Soils and Foundations* **43**(5), 149–159.
- Ishihara, K. and Okada, S. [1978] “Effects of stress history on cyclic behavior of sand,” *Soils and Foundations* **18**(4), 31–45.
- Idriss, I. M. and Boulanger, R. W. [2008] *Soil Liquefaction During Earthquakes* (Earthquake Engineering Research Institute, Oakland, CA).
- Mulilis, J. P., Arulanandan, K., Mitchell, J. K., Chan, C. K. and Seed, H. B. [1977] “Effects of sample preparation on sand liquefaction,” *Journal of the Geotechnical Engineering Division* **103**(2), 91–108.
- Nemat-Nasser, S. and Tobita, Y. [1982] “Influence of fabric on liquefaction and densification potential of cohesionless sand,” *Mechanics and Materials* **1**(1), 43–62.
- Oda, M. [1972] “Initial fabrics and their relations to mechanical properties of granular material,” *Soils and Foundations* **12**(1), 17–36.
- Oda, M., Kawamoto, K., Suzuki, K., Fujimori, H. and Sato, M. [2001] “Microstructural interpretation on liquefaction of saturated granular soils under cyclic loading,” *Journal of Geotechnical and Geoenvironmental Engineering* **127**(5), 416–423.
- O’Sullivan, C. [2011] *Particulate Discrete Element Modelling* (Spon Press, Oxon, UK).

- Satake, M. [1982] "Fabric tensor in granular materials," *IUTAM Symp. Deformation and Failure of Granular Materials*, Delft, pp. 63–68.
- Sitar, N. [1983] "Slope stability in coarse sediments," *Special Publication on Geological Environment and Soil Properties*, ed. R. N. Yong (ASCE, Reston, VA), pp. 82–98.
- Sitharam, T., Vinod, J. and Ravishankar, B. [2009] "Post-liquefaction undrained monotonic behaviour of sands: Experiments and DEM simulations," *Géotechnique* **59**(9), 739–749.
- Šmilauer, V., Catalano, E., Chareyre, B., Dorofeenko, S., Duriez, J., Gladky, A., Kozicki, J., Modenese, C., Scholtès, L. and Sibille, L. [2010], *Yade Documentation*, Available at: <http://yade-Dem.org/doc/>.
- Suzuki, T. and Toki, S. [1984] "Effects of preshearing on liquefaction characteristics of saturated sand subjected to cyclic loading," *Soils and Foundations* **24**(2), 16–28.
- Sze, H. and Yang, J. [2013] "Cyclic loading behavior of saturated sand with different fabrics," *Proc. 18th Int. Conf. Soil Mechanics and Geotechnical Engineering*, Paris, France, pp. 1611–1614.
- Thornton, C. [2000] "Numerical simulations of deviatoric shear deformation of granular media," *Géotechnique* **50**(1), 43–53.
- Vaid, Y., Chung, E. and Kuerbis, R. [1989] "Preshearing and undrained response of sand," *Soils and Foundations* **29**(4), 49–61.
- Wang, G. and Wei, J. [2016] "Microstructure evolution of granular soils in cyclic mobility and post-liquefaction process," *Granular Matter* **18**(3), 1–13.
- Wang, G. and Xie, Y. [2014] "Modified bounding surface hypoplasticity model for sands under cyclic loading," *Journal of Engineering Mechanics* **140**(1), 91–101.
- Wei, J. and Wang, G. [2016] "DEM analysis of initial fabric effects on cyclic liquefaction resistance and post-liquefaction behaviors of sands," Submitted to *Géotechnique Letters*.
- Ye, B., Lu, J. and Ye, G. [2015] "Pre-shear effect on liquefaction resistance of a Fujian sand," *Soil Dynamics and Earthquake Engineering* **77**, 15–23.
- Ye, J. H. and Wang, G. [2015] "Seismic dynamics of offshore breakwater on liquefiable seabed foundation", *Soil Dynamics and Earthquake Engineering* **76**, 86–99.
- Ye, J. H. and Wang, G. [2016] "Numerical simulation of the seismic liquefaction mechanism in an offshore loosely deposited seabed," *Bulletin of Engineering Geology and the Environment* **75**, 1183–1197.
- Ye, J. H., Huang, D. and Wang, G. [2016] "Nonlinear simulation of offshore breakwater on sloping liquefied seabed," *Bulletin of Engineering Geology and the Environment* **75**, 1215–1225.
- Yimsiri, S. and Soga, K. [2010] "DEM analysis of soil fabric effects on behaviour of sand," *Géotechnique* **60**(6), 483–495.
- Zhang, J. and Wang, G. [2012] "Large post-liquefaction deformation of sand, Part I: Physical mechanism, constitutive description and numerical algorithm," *Acta Geotechnica* **7**(2), 69–113.